ELSEVIER

Ceramics International 30 (2004) 417–427

CERAMICS INTERNATIONAL

www.elsevier.com/locate/ceramint

Fabrication and sintering characteristics of doctor blade YBCO-Ag tapes

L.C. Pathak

National Metallurgical Laboratory, MTP Division, Jamshedpur 831 007, India

Received 2 May 2002; received in revised form 10 November 2002; accepted 10 May 2003

Abstract

A detailed study of the fabrication and thermolysis behaviour of YBCO-Ag_x ($x=0.1$) tapes cast by doctor blade technique was carried out. During thermolysis, anisotropic shrinkage along the length and thickness of the tapes was observed due to the anisotropic nature of the capillary force acting on the particles during volatilization of the solvent, binder and plasticizer. The sintering study also revealed anisotropic behaviour along the thickness and length of the tapes. From the shrinkage and densification studies, the average activation energy was estimated to be ≈150 kJ/mol. However, it appears that two stages of sintering mechanisms operate one below ~1050 K (activation energy, $Q=52\pm0.5$ kJ/mol) and the other above 1050 K ($Q=301\pm6$ kJ/mol). Enhanced grain-growth after achieving a densification of 80% of the theoretical density was noticed. The sintering studies of the tapes along their thickness resulted in an apparent activation energy for sintering as 816±69 kJ/mol above 1193 K. Scanning electron microscopy studies indicated the possibility of liquid phase sintering above 1193 K, which was the cause of high activation energy.
© 2003 Elsevier Ltd and Techna S.r.l. All rights reserved.

Keywords: A. Tape casting; A. Drying; A. Sintering; D. Oxide superconductors; YBCO

1. Introduction

Doctor blade tape casting is widely used for the fabrication of two-dimensional specimens. In this method, either the doctor blade containing slurry moves over the carrier sheets or the carrier sheets move below the doctor blade. Amongst the several parameters, the selection of solvent, binder, defloculating agent, dispersing agent, plasticizer and carrier sheet are important for the efficient tape casting technique. Besides those parameters, the preparation of slurry, casting of tapes and drying of the tapes by evaporation of solvent are also important for the fabrication of good quality tapes. The subsequent processing of the unsintered (green) tapes often determines the usability of the final product. Fabrication of green tapes by varying the solvent, binder, plasticizer and deflocculating agents are extensively investigated [1–4]. Recently, binder removal characteristics are reported in the literature [5–6], however, the issues related to dimensional changes of the tapes during binder removal and shrinkage characteristics of the green tapes at elevated temperatures are not studied systematically. In this paper, the dimensional changes of the doctor blade cast Y–Ba–Cu-oxide (YBCO) tapes during different stages of processing are investigated.

In the last decade, extensive research activities have been carried out on the high temperature superconductors, particularly the YBCO and Bi–Pb–Sr–Ca–Cu-oxide for applications in various filed of engineering. The applications of these bulk high-temperature superconductors in electric motors [7], bearings [8–10], flywheel [10,11] and persistent current switch [12] are recently reported. The superconducting tapes applications in magnetic shielding are a distinct possibility. So far fabrication of YBCO superconducting tapes by doctor blade has been investigated [13–15] and none has studied the thermolysis and sintering behaviour of the green tapes.

In this paper, the fabrication of YBCO tapes by doctor blade casting technique, the thermolysis behaviour of the green tapes and the subsequent high temperature processing of the tapes are discussed.

E-mail address: lokesh@csnml.ren.nic.in (L.C. Pathak).

0272-8842/$30.00 © 2003 Elsevier Ltd and Techna S.r.l. All rights reserved.
doi:10.1016/S0272-8842(03)00126-3

2. Experimental

Submicrometre sized YBCO powder having nominal composition of $YBa_2Cu_3O_xAg_{0.1}$ (YBCO-Ag) was prepared by a chemical pyrophoric process. The starting materials were Y_2O_3 [99.9%][1]; $Ba(NO_3)_2$ [99%][2]; $Cu(NO_3)_2$, $3H_2O$ [99.5%][2] and $AgNO_3$ [99.5%][2]. The YBCO powder preparation technique has been reported elsewhere [16]. Silver (10 mol%) was added to help densification and to improve superconducting properties. From our earlier observation, it was noticed that the addition of silver helps in densification of YBCO superconductors provided the silver concentration, x, is $0 < x \leqslant 60$ (x in mol%) [17]. The pyrophorically generated powder was calcined at 1083 K for 12 h and the X-ray diffraction (XRD) analysis of the calcined powder was carried out by Phillips PW 1540 X-ray diffractometer using Ni filtered CuK_α radiation. The calcined powder was then used for the tape casting technique using a doctor blade.

The slurry for the tape casting was prepared by dispersing 25 g of the YBCO-Ag powder in an azeotropic mixture of methyl ethyl ketone (12 c.c.) and ethyl alcohol (6 c.c.) to which 6 drops of Emphos-PS21A (Wittco Chemical, USA) had been added as dispersing agent. The mixture was ball milled for 20 h and with this suspension, 2.5 g of binder [polyvinyl butyral (PVB)], 1.5 g of plasticizer [polyethylene glycol (PEG)] and 1.5 g of deflocculating agent [di-butyl pthalate (DBP)] were added and it was further ball milled for 20 h. The resultant slurry was de-aired to remove the trapped air bubbles and was cast on smooth PET sheets using a doctor blade. The removal of trapped air is necessary otherwise it will result in the formation of blistering during thermolysis of the tapes. In this tape casting method, the slurry containing doctor blade was moved over a carrier sheet. It is well known that in the tape casting process, the supports or carrier sheets are of prime importance, where the wetting of the support by the slurry is essential for good adherence. However, strong adherence of support and dried tapes also creates difficulty in stripping of the tapes from the support. In the present investigation, polyethylene (PET) sheet was found to be a good support.

It is also understood that non-uniform evaporation of solvent during drying of the tapes may lead to segregation of the particles resulting in the variation of density. To avoid this problem, a metal box was used to cover the tapes after the casting and the metal box had a small hole at the bottom of a side that allowed slow evaporation of the solvent. The cast tapes were dried for 24 h by this controlled evaporation of the organic solvent. The dried tapes were cut into the required shape for characterization. A detailed flow chart of the tape casting process is given in Fig. 1. The apparent densities of the green tapes were determined from the mass and the apparent volume of the green tapes cut across the length. The reported values of the green densities are the average value of five measurements along the green tapes. The green tapes cut along the lengths were also calcined at 1203 K for 10 h in air to study the uniformity of the organic components in the green tapes. Five cut pieces were used for the measurement of average weight loss.

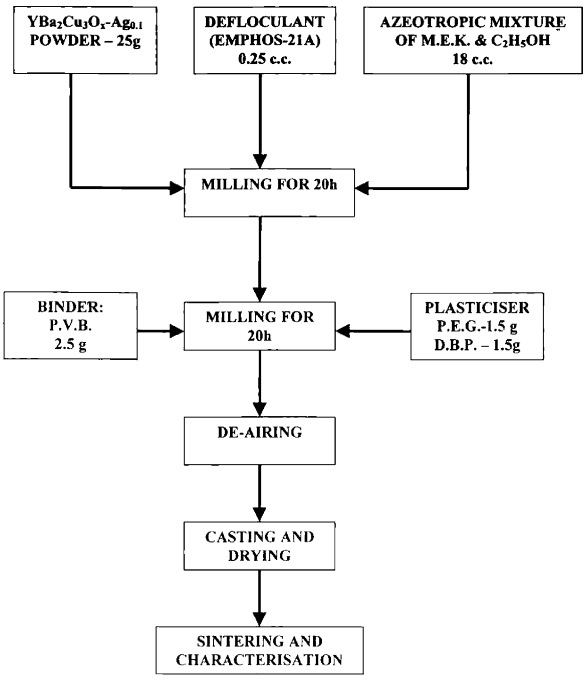

Fig. 1. Flow chart for the tape casting of YBCO-Ag powders.

One of the important steps for the tape casting technique is burning out of the organic components during thermolysis process. In this investigation, the thermolysis behaviour of the cast tapes was studied by using TG/DTA and thermo-mechanical analyzer (TMA). The TG/DTA was used for the study of weight loss and thermal behaviour of the specimens during heating. The TG/DTA experiments of the green tapes were carried out from 300 to 773 K by a thermal analyzer, STA 625 (Stanton Radcroft, UK). The TMA (DT30, Shimadzu, Japan) was used to measure the dimensional changes of the samples during heating or cooling cycles. Since it was difficult to measure the shrinkage of the tapes along the lengths using TMA, the lengths of the tapes were measured manually. For this, rectangular pieces of the YBCO green-tapes were heated at the rate of 60 K/h and the lengths of the tapes were measured at regular interval of temperatures and isothermally hold for a minutes. During sintering of the tapes, 1 mm thick and flat platinum plate with smooth surface was used to support the YBCO-Ag tapes and the platinum plate was placed on a flat alumina slab.

[1] Indian Rare Earth Limited.
[2] Merck India Limited

Prior to the sintering studies, the rectangular pieces of the green tapes were calcined at 873 K for 10 h in air. Subsequently, the sintering studies in air atmosphere were carried out by heating the tapes at several temperatures ranging between 873 and 1253 K. The samples were isothermally held for 10 h and the accuracy of the temperature measurement was ± 1 K. The heating rate was 60 K/h from room temperature to 873 K then 300 K/h to the final temperature. The change of length of the samples was measured before and after each sintering. The sintered samples were polished and etched by 0.001% hydrochloric acid solution in ethanol for 2 min and washed with ethanol. A short period of etching was adopted here to minimise the preferential etching of the constituents. The etched samples were studied by scanning electron microscope (SEM) (CAM SCAN, UK). Average grain sizes of the sintered specimens were determined from the scanning electron micrographs of the etched surfaces. The variation of length with sintering time was also been measured at different temperatures to evaluate the sintering kinetic parameters. The error in length measurement was $\approx \pm 1\%$ in all cases.

Sintering studies of the YBCO-Ag tapes were also investigated along the thickness of the doctor blade cast tapes using TMA. The samples were held at several isothermal temperatures in the range of 1193–1218 K for 30 min. The apparent densities of the sintered samples were measured by Archimedes principle of liquid immersion technique. The accuracy for the density measurement was estimated to be $\pm 1\%$. The true densities of the samples were also measured by liquid penetration technique where the liquid was allowed to penetrate into the open pores. Green YBCO tapes were also sintered at different temperatures for 1 h in air and were subsequently oxygenated at 773 K for 20 h. The superconducting properties of the oxygenated samples were also measured with the help of closed cycle He cryo-cooler (APD Cryogenics, USA). Critical current densities were measured at 77 K using linear four-probe method, with 1 μV/cm criteria.

3. Results and discussion

3.1. Thermolysis characteristics of YBCO-Ag green tapes

The dried green tapes of YBCO-Ag superconductors were flexible due to the presence of a polymeric network and these green tapes had an average density of 2.56 g cm^{-3}. The polymeric content was estimated from the weight loss of the tapes after calcination at 1203 K for 10 h and found to be 32.5%. The thermal analysis (TG/DTA) of the green tapes (Fig. 2) revealed that the mass loss from the tapes occurred in two steps. The first step of mass loss due to the evaporation loss of the organic solvent (MEK and ethanol), dispersion agent and

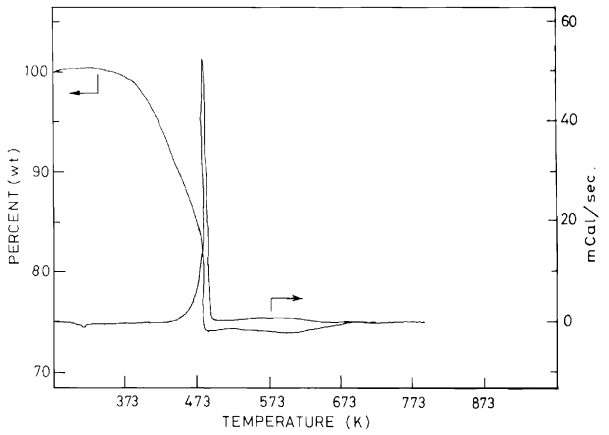

Fig. 2. TG/DTA thermogram of the green YBCO-Ag tapes showing the exothermic peak during evaporation of organic materials.

deflocculant (DBP) from the green tapes was observed to start at ~353 K The TG plot also revealed a sharp weight loss at ~473 K due to removal of polymeric substances from the tapes in the second step. The weight loss in the second step was also associated with an exothermic peak in the DTA thermogram. Subsequently the weight loss from the tapes became almost constant up to 773 K. From the TG/DTA plot it was estimated that ~13% weight loss took place in the first step and ~12.5% weight loss was accounted for in the second step. This estimated weight loss in the second step was consistent with the total weight of the binder and plasticizer. Therefore, the DTA peak and the sharp weight loss in the TG thermogram indicated the removal of binder/plasticizer from the tapes. The total weight loss from the tapes during removal of solvent and organic materials was found to be 25.5%, which was lower than the total weight loss of 32.5% after calcination at 1203 K. This excess loss of mass was due to further loss of mass above 773 K and could be understood from the phase analyses of the tapes.

The phase analyses of the tapes heated at different stages of processing were studied by the X-ray diffraction technique. The XRD patterns of the calcined YBCO-Ag powder and the processed tapes are shown in Fig. 3. From the XRD patterns it could be observed that the calcined powder contain orthorhombic 123 as the main phase in the pattern (peaks due to Ag overlaps with the 123 peaks), whereas, significant amount of $BaCO_3$, Y_2O_3 and CuO phases were observed in the green tapes. This implies that degradation of YBCO-Ag powder had taken place during slurry preparation. The excess weight loss from the tapes above 773 K was due to decomposition of $BaCO_3$. The weight loss due to presence of some polymeric residue that burned out at elevated temperature also cannot be ruled out.

The thermo-mechanical analyses of the tapes representing the variation of thickness and the measurement of tapes length indicated that the weight loss from the

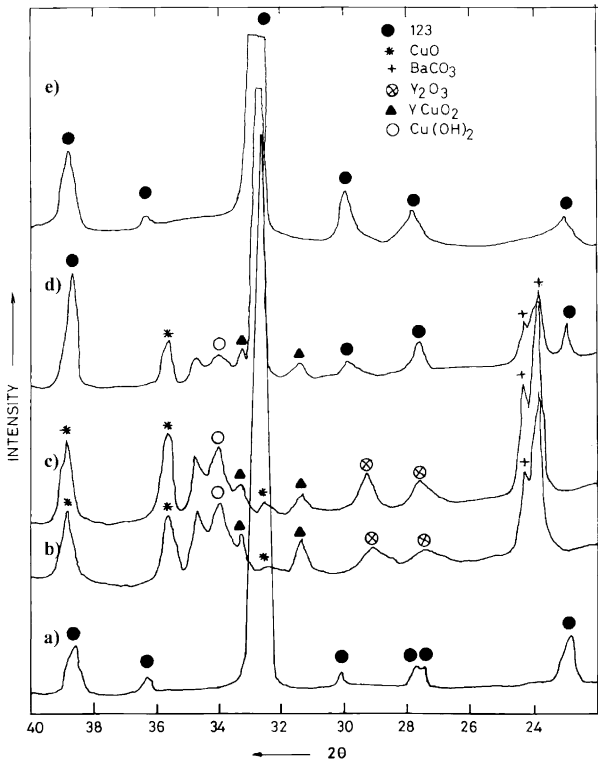

Fig. 3. XRD patterns of the specimens: (a) single phase 123 powder before tape casting and YBCO tapes heated at various temperatures for 10 h, (b) 873 K, (c) 1073 K, (d) 1173 K and (e) 1193 K.

specimens was associated with the dimensional shrinkages of the tapes during thermolysis process. A typical TMA curve of the tape is shown in Fig. 4 and the shrinkage curve along the length of the tape is given in Fig. 5. From the shrinkage study along the thickness of the tapes (Fig. 4 showing the variation of shrinkage and its derivative with the heating times), it appeared that the tapes underwent three steps of shrinkages during the heating process. The first step of shrinkage (~1%) at 333 K represented the glassy transition (softening) of the polymers, whereas, the second step represented the evaporation-assisted shrinkage of ~0.5% (due to volatile materials) at 558 K and the third step of shrinkage at 800 K was due to removal of carbonaceous materials followed by the densification of the tapes. The total shrinkage along the thickness was found to be ~2% below 873 K i.e. during the binder removal stage. The shrinkage curve along the length of the tapes showed shrinkage of 19.5% below 873 K. This indicates that the shrinkage of the tapes along the length of the tapes was more than the thickness direction. Explanation for the anisotropic shrinkage behaviour follows:

It is well known that during drying of the tapes, two stages of drying processes that include evaporation of solvent and evaporation/sublimation of polymeric materials takes place. The capillary migration of the solvent and binder from the surface of the tapes will create a capillary force, F, upon the particles and can be expressed as [18].

$$F = -2\gamma \mathrm{lv}/r$$

where, γ_{lv} is the surface tension and r is the radius of the curvature of the capillary. A schematic representation of the tapes and the capillary forces acting on different directions are shown in Fig. 6.

Let us consider a geometry of the tape as shown in the figure (Fig. 6), where point O indicates the center of the tape, thickness of the tape AE = t, width of the tape AB = w and length of the tape AD = l. For any tape, $l >> w >> t$. It is understood that the organic materials (binder, plasticiser, deflocculating agent, solvent etc.) evaporate from the outer surface through capillaries and attractive capillary forces on the adjacent particles will be created during mass transfer. For any gas to evaporate from the center of the tapes i.e. point O, it has to traverse a distance of $l/2$, $w/2$, and $t/2$ for its evaporation along X, Y and Z direction respectively. Since, $l >> w >> t$, the gas at the center will have more probability to evaporate along the Z direction than other two directions due to easy escape nature of fluid. This suggests that the number of capillaries per unit area in the ABCD plane will be more than AEFD or DFGC planes. Moreover, the area of ABCD plane is larger than AEFD or DFGC planes. Therefore, total evaporation loss will be more from the ABCD plane than either AEFD or DFGC planes. Since the capillary force is perpendicular to the mass flow, the particles of the tapes will experience more attractive force perpendicular to the thickness of the tapes i.e. X and Y direction. Similarly, the evaporation loss from AEDF will be more in comparison to the DFGC plane. This evaporation from the AEDF will create attractive forces along the X and Z direction. If we take all the capillary forces in account, the total attractive force will be more along the X direction compared to the Y and Z directions. This attractive force brings the ceramic particles together and also gives sufficient handling strength to the fragile tape. The total shrinkages of the YBCO-Ag tapes were found to be 19% along the thickness direction after 1 h holding at 1203 K and 30% along the length after 10 h sintering at 1203 K. The TMA and longitudinal shrinkage data indicated that at high temperature the shrinkage due to sintering was less along the thickness of tapes (~17%) than in the length of the tapes (~30%). This is possibly due to presence of more porosity along the length of the tapes. These pores are due to the space left over by the capillaries during binder removal. However, a further discussion on the sintering and grain-growth characteristics of these YBCO-Ag tapes follows.

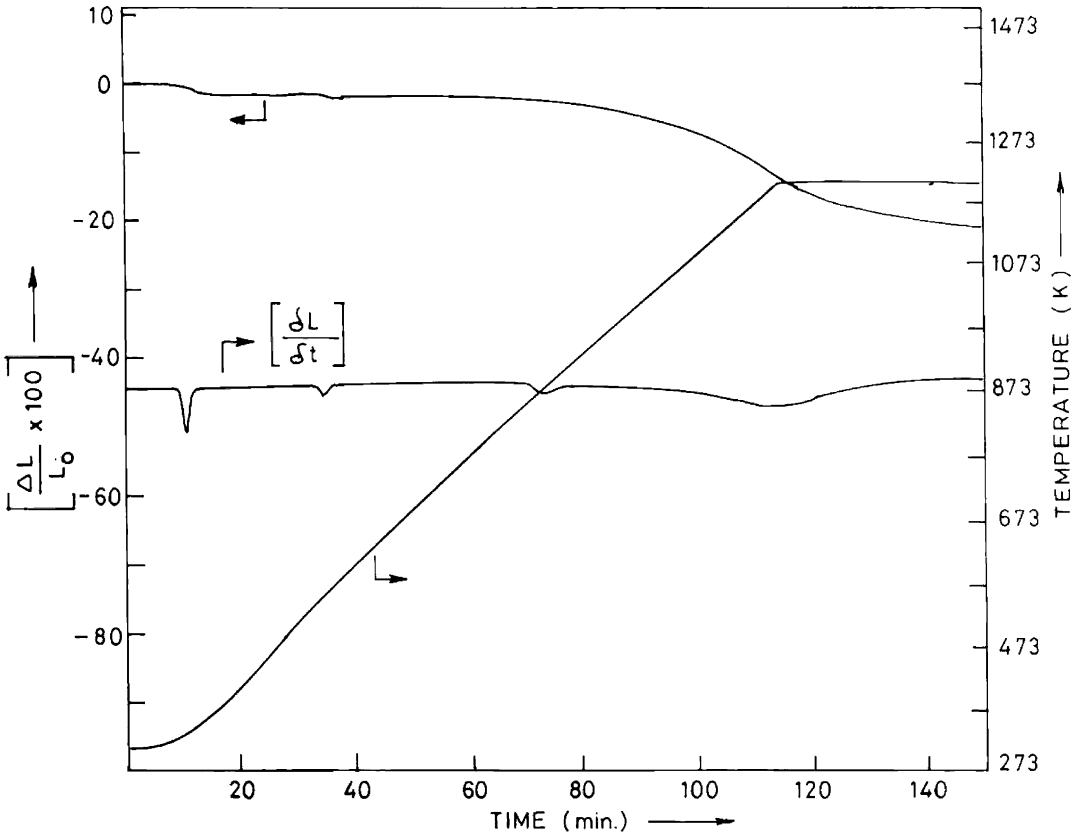

Fig. 4. Thermo-mechanical analyzer plot showing the variation of the thickness of YBCO-Ag tapes with temperatures during thermolysis of green tapes.

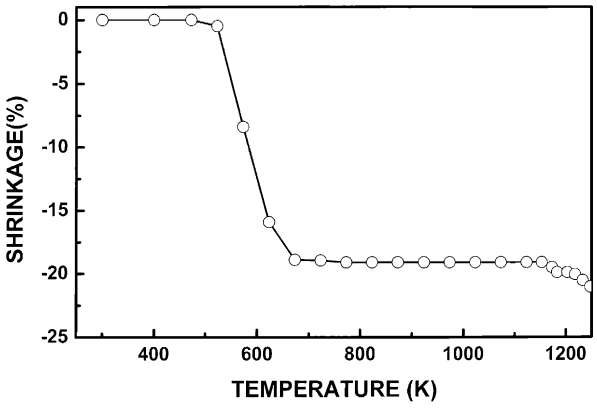

Fig. 5. Variation of the length of YBCO-Ag tapes with temperatures during thermolysis of green tapes.

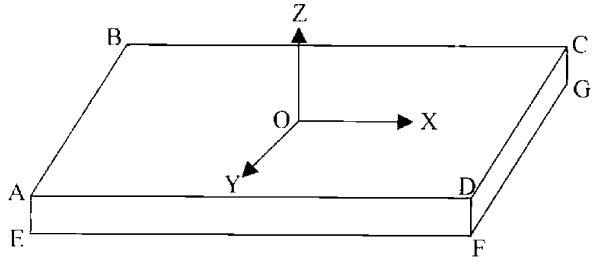

Fig. 6. Schematic of the YBCO-Ag green tapes with a dimension of $l \times w \times t$..

3.2. Sintering and densification characteristics of the YBCO-Ag tapes

The densification or sintering of any sample is related to the dimensional shrinkage occurring in the samples during sintering and the linear shrinkage parameter, $\delta L/L_o$ (α) is time and temperature dependent because of the systematic decrease of porosity of the compacts with the sintering time and temperatures. The parameter, α can also be expressed as a function of time (t) and temperature (T in K) [19]

$$\alpha = \frac{\Delta L}{L_o} = \left(\frac{K\gamma\Omega D_0 e^{-\frac{Q}{kT}}}{kTr^p}\right)^m t^m \quad (2)$$

where, ΔL is the change in length of the specimen after a time interval of t, L_o is the initial length, K, p, m are numerical constants, γ is the surface energy, Ω is vacancy volume, k is the Boltzman's constant, T is absolute temperature and r is the particle radius, Q is the activation energy for sintering and D_o is self-diffusion coefficient at zero Kelvin. For a fixed particle size and single mechanism, γ, Ω, r and D_o become constant.

For any isothermal temperature, the slope of the log ($\alpha^{1/m}$) with log (time) plot gives the value of sintering kinetic parameter, m. The slope of the $\ln(\alpha^{1/m}T/t)$ with inverse of temperature plot gives the value of apparent

activation energy for sintering. The sintering characteristics of the YBCO-Ag tapes along the length and thickness of the tapes are discussed separately.

3.2.1. Sintering YBCO-Ag tapes along the length

The variation of total shrinkage experienced by the tapes along the direction of its length is shown in Fig. 7. The tapes were sintered at temperatures ranging from 873 to 1253 K and soaked for 10 h in air. The isothermal shrinkage variations with sintering time were measured at several temperatures. A few representative shrinkage plots with sintering times are given in Fig. 8. The variation of linear shrinkages showed a continuous increase of shrinkage parameters with sintering temperatures and times (Fig. 8). It was also noticed from the logarithmic variations of shrinkages with times (Fig. 9) that the kinetic parameter, m, decreases marginally with the increase of sintering temperatures from 0.52 at 903 K to 0.49 at 1093 K and finally 0.47 at 1203 K. This decrease of m is possibly due to a change of sintering mechanism [20]. The correlation factor for the linear fitting is found to be ~99.5% for all these curves. The apparent activation energies for sintering were estimated from the plot of $\ln(\alpha^{1/m}T/t)$ with $1/T$ (Fig. 10). The plot clearly indicated two different slopes for sintering, one below 1050 K and the other above 1050 K. The activation energy, Q_2, was found to be 301 ± 6 kJ/mol above 1050 K, whereas, 52 ± 0.5 kJ/mol was estimated to be the activation energy Q_1 below 1050 K. These changes of activation energies and kinetic parameters, clearly suggest two stages of sintering for YBCO-Ag tapes. One of the possibilities for the low value of activation energy, Q_1 at low temperature regime is due to presence of unreacted phases in the YBCO-Ag tapes. Similar observations were also been noticed during sintering of unreacted YBCO powders [21]. However, the activation energy below 1050 K was much lower than the reported value of 627 kJ/mol for

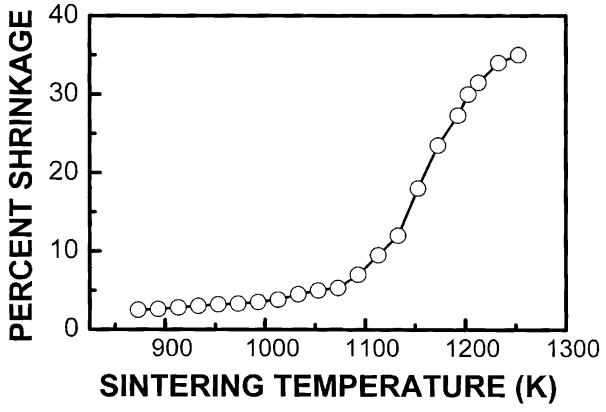

Fig. 7. Variation of linear shrinkage along the tapes length with sintering temperatures for the YBCO-Ag tapes sintered at several isothermal temperatures.

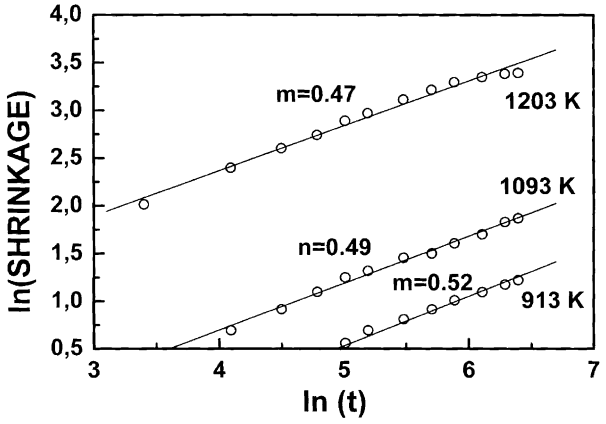

Fig. 9. Logarithmic variation linear shrinkages (along the tapes length) with the logarithmic values of the sintering times for the YBCO-Ag tapes sintered at several isothermal temperatures.

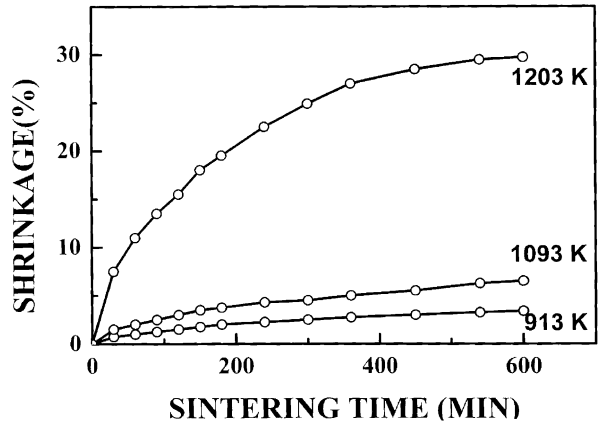

Fig. 8. Variation of linear shrinkage along the tapes length with sintering time for the YBCO-Ag tapes sintered at several isothermal temperatures.

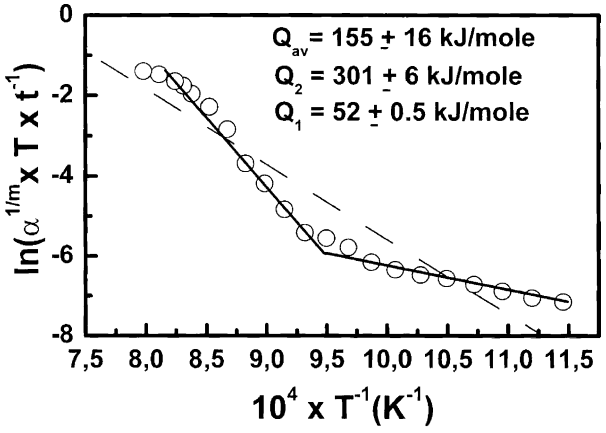

Fig. 10. Arrhenius plot for the estimation of activation energy for sintering of the YBCO-Ag tapes. Q_1 is the activation energy below 1050 K, Q_2 is the activation energy above 1050 K and Q_{av} is the average activation energy.

the unreacted YBCO powder. Therefore, the possibility of other mechanism for the low activation energy cannot be ruled out. The activation energy Q_2 is due to reaction aided sintering mechanism. A value of 383 kJ/mol was reported to be the activation energy for reactive sintering of YBCO powder [13]. The presence of impurities or high defect concentration is a possible reason for lowering of the activation energy above 1050 K. However, it is difficult to predict the exact mechanism for lowering activation energies in low and high temperature regime. The average activation energy for sintering (Q_{av}) was estimated to be 155±16 kJ/mol. The dashed line in Fig. 10 was used for the estimation of average activation energy for sintering.

3.2.2. Densification behaviour

In ceramics, three types of densities: apparent density, true density and theoretical density are known and all these densities have useful significance in understanding the densification behaviour. The open pores and close pore volumes are included with the materials volume to calculate the apparent density of the specimens, whereas, only the close pore volume is included with the material volume to obtain the true density. The theoretical density is calculated from the molecular mass and the unit cell volume obtained from the X-ray diffraction analyses. Fig. 11 showed the variation of true and apparent density with sintering time for the YBCO-Ag tapes sintered at 1203 K. From the figure (Fig. 11b) it is evident that the true density initially increased and then decreased. The increase of true density was due to channelization of pores and then decreased as the pore started closing and eliminated in the final stage of sintering. The SEM studies (Fig. 14b and c) showed the channelization and rounding off pores. Expectedly, the density versus sintering time plot (Fig. 11a) showed a continuous increase of apparent densities with the sintering times (Fig. 11). The variation of apparent densities with sintering temperatures were also measured for the tapes sintered at various temperatures for a fixed period of 10 h and plotted in Fig. 12, which showed a maximum densification of 6.3 g cm^{-3} at 1253 K. Densification behaviour was also used for understanding the sintering mechanism and can be expressed by using a simplified sintering theory [22,23] as,

$$\frac{dg}{dt} = \frac{K'}{T} D_o e^{\frac{-Q_D}{kT}} \quad (3)$$

where, dg/dt is the rate of densification, k' is the rate constant, T is the temperature, D_o is the diffusion constant, Q_D is the activation energy for sintering and k is the Boltzman constant. By plotting $\ln(T \times dg/dt)$ with the inverse of temperatures, the apparent activation energy for sintering is calculated to be 147±2 kJ/mol (Fig. 13). Though the shrinkage study along the length of the tapes indicated two stages of sintering, the densification analysis apparently revealed only one mechanism. However, a careful investigation into the experimental data

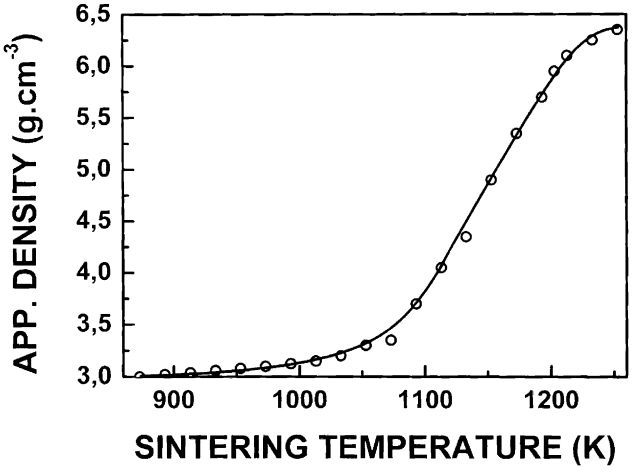

Fig. 12. Variation of apparent densities with the sintering temperatures for the YBCO-Ag tapes sintered at several isothermal temperatures for 10 h.

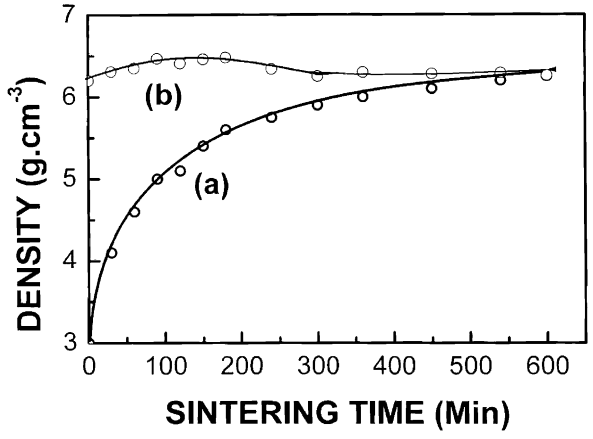

Fig. 11. Variation of densities with the sintering time for the YBCO-Ag tapes isothermally sintered at 1203 K. (a) Apparent density and (b) true density.

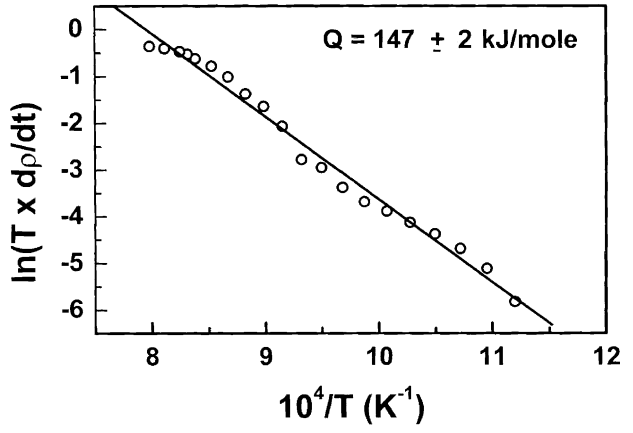

Fig. 13. Arrhenius plot for the estimation of activation energy for sintering of the YBCO-Ag tapes form the densification data.

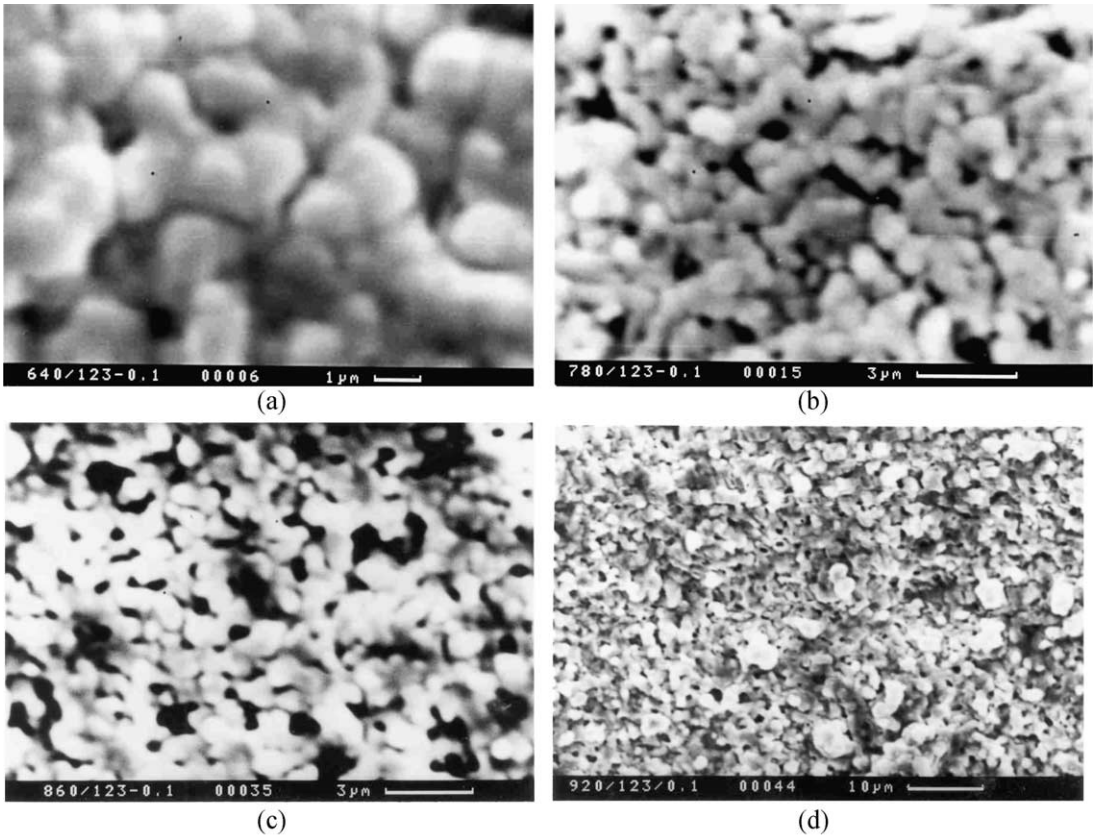

Fig. 14. Scanning electron microscopy images of the YBCO-Ag tapes isothermally sintered for 10 h at (a) 913 K, (b) 1053 K, (c) 1133 K and (d) 1193 K.

also revealed the possibility of two stage of densification. The average value of the activation energy for sintering obtained from the sintering study was 155 ± 16 kJ/mol, which is comparable with the estimated value of activation energy from the densification curve. The closeness of the activation energies values obtained from the shrinkage and densification studies indicated one mechanism operating for the sintering of these tapes.

3.2.3. Grain-growth characteristics

It is well known that the grain-growth is always associated with the densification of any material during sintering. The grain-growth characteristic of these YBCO-Ag tapes was also investigated in the present investigation. Fig. 14 showed some representative SEM micrographs of the YBCO-Ag tapes sintered at different temperatures and soaked for a fixed period of 10 h. The SEM studies revealed the compact microstructures at low temperatures (Fig. 14a) and as the temperature increased the appearance of open pores were distinctly visible (Fig. 14b). The opening up of the pores was due to sintering of agglomerated particles, which also resulted in the formation of some rounded pores. As the sintering temperature increases further, more pores opened up and formed pore channels (Fig. 14c). At higher temperatures those open pores started rounding off to closed pores during sintering and more and more closed pores appeared (Fig. 14d). The average grain size was estimated from the micrographs using line intercept method. The variation of the average grain size with sintering temperature is presented in Fig. 15. From Figs. 12 and 15, it appears that the grain growth accelerated after the densification had reached a value of 80% of the theoretical density (6.35 g cm^{-3}).

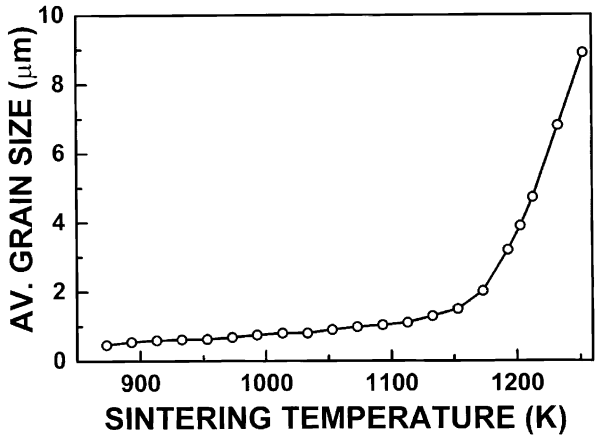

Fig. 15. Variation of average grain size of the sintered YBCO-Ag tapes with sintering temperatures.

3.2.4. Sintering characteristics along the thickness of the tapes

As discussed earlier, the shrinkage along the thickness of the tapes was investigated by TMA and a typical TMA curve was also shown in Fig. 4. The variation of the sintering parameter, α, with sintering time was plotted in Fig. 16, which also showed the continuous increase of shrinkage parameters with sintering times and temperatures. From the figure (Fig. 16) it was observed that the YBCO-Ag tapes experience shrinkage of 19.6% after sintering at 1218 K. The corresponding logarithmic variation of shrinkage with log time was plotted in Fig. 17, which indicated a change of the slopes with the increase of sintering temperatures. The value of sintering kinetic parameter, $m = 0.27$ was obtained at 1193 K, which decreased to 0.12 at 1218 K. The variation of sintering kinetic parameter, m with sintering temperature is given in Fig. 18. The observed decrease of kinetic parameter was due to reduction of driving force for sintering. Moreover the sintering studies along the thickness of the tapes were possibly carried out in the final stage of sintering, where the pores have started closing. This will reduce the driving force for sintering and changes the mechanism and possibly increase the activation energy for sintering. A SEM image of the tape sintered at 1213 K is shown in Fig. 19, which showed the existence of closed pores in these tapes. The microstructure also reveals the possibility of liquid phase sintering for these tapes. Since the sintering studies of YBCO-Ag superconductors was reported to take place by a liquid phase sintering method above 1193 K [17], the occurrence of liquid phase during sintering could not be ruled out. The Arrhenius plot for the estimation of apparent activation energies is given in Fig. 20 and the slope of the straight line yields the apparent activation energies as 816 ± 16 kJ/mol. The high value of the activation energies for sintering as obtained by the TMA study along the thickness is possibly due to liquid phase sintering or due to final stage of sintering.

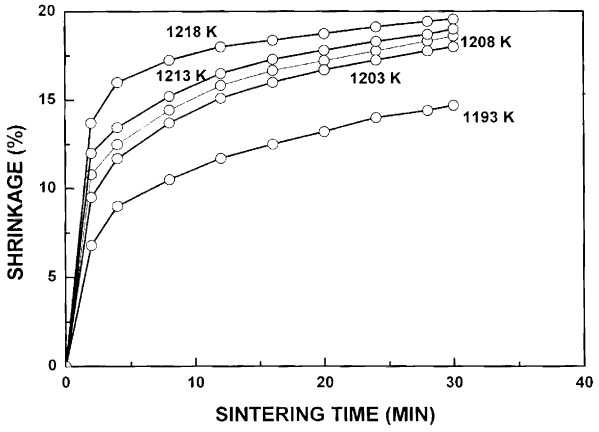

Fig. 16. Variation of linear shrinkage for the YBCO-Ag tapes along its thickness with sintering time. Tapes were also sintered at several isothermal temperatures.

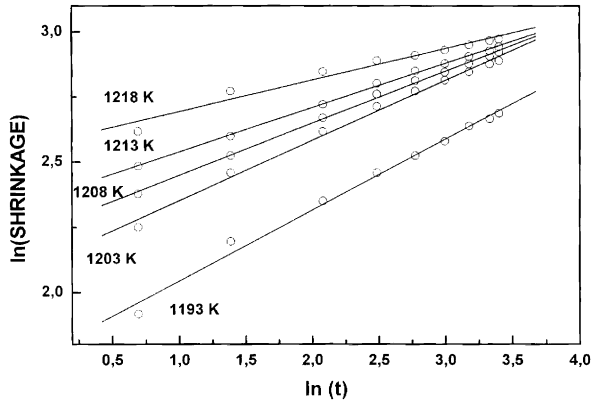

Fig. 17. Logarithmic variation of linear shrinkage along the thickness of the tapes with the logarithmic value of the sintering time for YBCO-Ag tapes sintered at several isothermal temperatures.

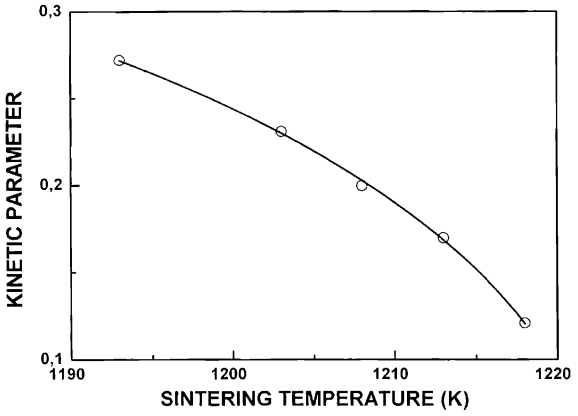

Fig. 18. Variation of sintering kinetic parameter with the sintering temperatures for the YBCO-Ag tapes isothermally sintered at temperatures between 1193 K and 1218 K.

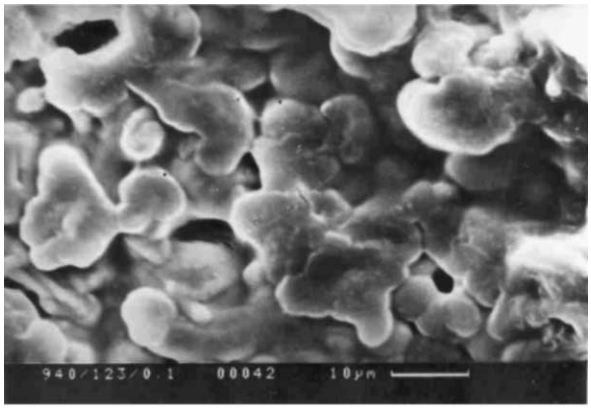

Fig. 19. Scanning electron micrograph of the YBCO-Ag tapes sintered at 1213 K.

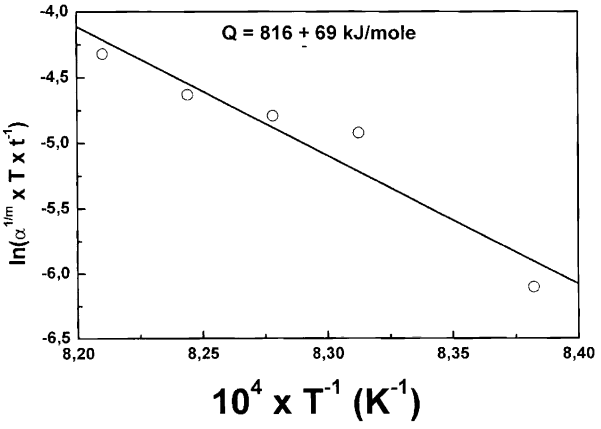

Fig. 20. Arrhenius plot for the estimation of activation energy for sintering of the YBCO-Ag tapes isothermally sintered at temperatures between 1193 K and 1218 K.

3.3. Transport properties of the tapes

It was observed from the measurements of transport properties that the critical current density in zero magnetic field for these sintered YBCO-Ag tapes were very low and a maximum value of ~1000 A/cm^2 is achieved at 77 K. The variations of the superconducting properties of YBCO-Ag tapes sintered at different temperatures are presented in Table 1. The T_c onset was observed at ~94 K for all the cases and the variation of ΔT_c was primarily due to weak-link across the grain boundaries [24]. The lowering of room temperature resistivity and the transition width and the increase of transition temperatures with the increase of sintering temperatures was due to higher densification. The J_c values reported in the table are the average value of 3 identically processed tapes without having any visible defects. The observed decrease in the J_c and T_c values and the increase of transition width above 1223 K was due to melting of silver and wetting of YBCO grains resulting in the decomposition of 123 phase. The lowering of transport properties is consistent with our earlier observations [17].

Table 1
Superconducting properties of YBCO-Ag tapes sintered for 10 h at various temperatures and oxygenated at 773 K for 20 h

Sintering temperature (K)	1153	1173	1193	1213	1223	1233	1253
Resistivity at 300 K×10^3 (Ω cm)	6.28	4.19	1.6	0.43	0.29	0.51	1.23
Transition temperature (K)	88.1	91.3	91.5	92.0	92.4	91.8	88.5
Transition width [ΔT_c (K)]	5.5	2.6	2.2	2.3	2	2.5	5.3
Critical current density (A/cm^2) at 77 K	11	143	400	800	1012	712	623

4. Conclusions

The fabrication of YBCO-Ag tape by doctor blade technique and subsequent processing of the cast tapes was investigated. The thermolysis behaviour of the green tapes showed anisotropic behaviour due to more capillary force along the length of the tapes than the thickness of the tapes. The sintering studies indicated two stages of sintering mechanisms operating the system. From the shrinkage behaviour, the activation energy for sintering was estimated to be 301±6 kJ/mol above 1050 K and 52±0.5 kJ/mol below 1050 K. The average activation energy for sintering was calculated to be ≈150 kJ/mol from the shrinkage and densification behaviour. Enhanced grain-growth after achieving a densification of 80% of the theoretical density was noticed. The sintering studies of the tapes along its thickness resulted an apparent activation energy for sintering as 816±69 kJ/mol above 1193 K. Scanning electron microscopy studies indicated the possibility of liquid phase sintering above 1193 K, which is the cause of high activation energy.

Acknowledgements

The author wants to thank Dr. S.K. Mishra (Pathak), National Metallurgical Laboratory, Jamshedpur, Professor K.L. Chopra and Professor D. Bhattacharya, Materials Science Centre, Indian Institute of Technology, Kharagpur, India for their valuable help in carrying out this work.

References

[1] M.J. Cima, J.A. Lewis, A.D. Dovoe, J. Am. Ceram. Soc. 72 (1989) 1192.
[2] N. Das, H.S. Maiti, J. Membr. Sci. 140 (1998) 205.
[3] G.P. van der Beek, U. Gontermann-Gehl, E. Krafeczyk, J. Eur. Ceram. Soc. 15 (1995) 741.
[4] T. Chartiera, R. Penarroya, C. Pagnoux, J.F. Baumarda, J. Eur. Ceram. Soc. 17 (1997) 765.
[5] P. Calvert, M.J. Cima, J. Am. Ceram. Soc. 73 (1995) 575.
[6] A.L. Salam, D.R. Matthews, H. Robertson, J. Eur. Ceram. Soc. 20 (2000) 335.
[7] L.K. Kovalev, K.V. Ilushin, V.T. Penkin, K.L. Kovalev, A.E. Larionoff, S.M.-A. Koneev, K.A. Modestov, S.A. Larionoff, V.N. Poltavets, I.I. Akimov, V.V. Alexandrov, W. Gawalek, B. Oswald, G. Krabbes, Supercond. Sci. Technol. 15 (2002) 817.
[8] Y. Zhang, Y. Postrekhin, K.B. Ma, W.-K. Chu, Supercond. Sci. Technol. 15 (2002) 823.
[9] A.C. Day, M. Strasik, K.E. McCrary, P.E. Johnson, J.W. Gabrys,

J.R. Schindler, R.A. Hawkins, D.L. Carlson, M.D. Higgins, J.R. Hull, Supercond. Sci. Technol. 15 (2002) 838.
[10] K. Matsunaga, M. Tomita, N. Yamachi, K. Iida, J. Yoshioda, M. Murakami, Supercond. Sci. Technol. 15 (2002) 842.
[11] T.A. Coombs, A. Canstz, A.M. Campbell, Supercond. Sci. Technol. 15 (2002) 831.
[12] M. Tomita, M. Murakami, S. Nariki, K. Sawa, Supercond. Sci. Technol. 15 (2002) 846.
[13] H. Shimizu, H. Kumakura, K. Togano, Jpn. J. Appl. Phys. 27 (1988) L414.
[14] M. Ishii, X. Maeda, M. Matsuda, M. Takata, T. Yamashita, Jpn. J. Appl. Phys. 26 (1987) L1959.
[15] T. Konaka, I. Sankawa, T. Matsura, T. Higashi, K. Ishihara, Jpn. J. Appl. Phys. 27 (1988) L1092.
[16] D. Bhattacharya, L.C. Pathak, S.K. Mishra, D. Sen, K.L. Chopra, Appl. Phys. Lett. 57 (1990) 2145.
[17] L.C. Pathak, S.K. Mishra, D. Bhattacharya, K.L. Chopra, J. Mater. Res. 14 (1999) 4148.
[18] G.W. Sherer, J. Am. Ceram. Soc. 73 (1990) 3.
[19] D.L. Johnson, I.B. Cutler, J. Am. Ceram. Soc. 46 (1963) 541.
[20] L.C. Pathak, S.K. Mishra, S. Srikanth, J. Mater. Res. 17 (2002) 895.
[21] L.C. Pathak, S.K. Mishra, P.G. Mukunda, M.M. Godkhindi, D. Bhattacharya, K.L. Chopra, J. Mater. Sci. 29 (1994) 5455.
[22] J. Wang, R. Raj, J. Am. Ceram. Soc. 74 (1991) 1217.
[23] R.M. German, Sintering, in: Powder Metallurgy Science, Metal Powder Industries Federation, Princeton, NJ, 1994.
[24] L.C. Pathak, S.K. Mishra (Pathak), S.K. Das, D. Bhattacharya, K.L. Chopra, Physica C 351 (2001) 295.